



# UAV-aided bridge inspection protocol through machine learning with improved visibility images



Euisseok Jeong<sup>a,2</sup>, Junwon Seo<sup>b,1,\*</sup>, James P. Wacker<sup>c</sup>

<sup>a</sup> Dept. of Civil and Environmental Engineering, South Dakota State Univ., Brookings, SD 57007, USA

<sup>b</sup> ASCE Timber Bridges Committee, Dept. of Civil and Environmental Engineering, South Dakota State Univ., Brookings, SD 57007, USA

<sup>c</sup> Forest Service, US Forest Products Lab, One Gifford Pinchot Dr., Madison, WI 53726, USA

## ARTICLE INFO

### Keywords:

Drone  
Bridge inspection  
Damage quantification  
Image processing  
Visibility improvement  
Computer vision  
Machine learning  
Convolutional Neural Network (CNN)

## ABSTRACT

This paper aims to introduce a new bridge inspection protocol using Convolutional Neural Network (CNN)-based machine learning in conjunction with improved visibility images acquired by Unmanned Aerial Vehicles (UAVs). With two UAVs, separate inspections following the proposed protocol were initially performed indoor to quantify the damage state of three concrete columns and four Cross-Laminated Timber (CLT) beams. The protocol using the two UAVs was also adopted to inspect an in-service four-span timber bridge in Pipestone, Minnesota in the United States. During damage identification, various types of visually detected damage were classified through CNN-based machine learning. For image visibility improvement, each image with damage was processed with appropriate adjustment of brightness, contrast, and sharpness to identify and measure the damage in an efficient way. The proposed protocol was found to be capable of bridge damage identification and measurement with an average error of 9.12% when compared to the direct measurements.

## 1. Introduction

Regular inspections of deteriorating bridges are required to ensure their continued safe operation. These conventional inspections are based on visual techniques and face challenges on the cost-effective identification of damage located in inaccessible areas. In this case, bridge inspectors will likely access the damaged areas with specialized equipment such as snooper trucks which includes additional cost and safety hazards. Bridge inspections using Unmanned Aerial Vehicles (UAVs) can help resolve these challenges. Several recent studies (Cunningham et al., 2015; Duque et al., 2018a, 2018b; Hallermann & Morgenthal, 2014; Khaloo et al., 2018; Otero et al., 2015; Reagan et al., 2017b, 2017a; Seo et al., 2018a, 2018c, 2018b; Zink & Lovelace, 2015) have accounted for that a new inspection tool using UAVs can aid, or enhance, conventional bridge inspections. For instance, Seo, Duque, and Wacker (2018b) performed an on-site bridge inspection in South Dakota in the United States with a UAV to capture numerous images for all critical sections. It was found that the UAV was a reliable tool for the identification of several types of damage, including concrete efflorescence on the bridge.

Although the UAV-aided inspection can help improve the accessibility and cost-efficiency of a bridge inspection, there are still three areas that need improvements: 1) low-quality of images; 2) time-consuming damage classification; and 3) imprecise quantification of damage. The image quality improvement is a significant task necessary for both damage identification and quantification accurately. If a UAV operator captures poor quality photographs at low illumination such as inspection underneath a deck, it is inefficient for inspectors to identify and quantify the damage due to the low illumination images. Several studies (Gervaise et al., 2012; Inoue & Tajima, 1994; Kao et al., 2009; Nomura et al., 2008) have attempted to improve UAV image quality, in order to inspect bridges in an efficient way. Inoue and Tajima (1994) enhanced color image quality using three main factors, encompassing image sharpness, contrast, and saturation.

During the UAV-aided bridge inspections, a high number of inspection images are generally obtained. Examining each image to identify and classify the damage may be a cumbersome task requiring an enormous amount of effort and time. To overcome this issue, the machine learning technique has been used for damage classification in different areas (Dick et al., 2019; Gulgec et al., 2019; Park et al., 2019; Yang et al.,

\* Corresponding author.

E-mail addresses: [Euisseok.Jeong@sdstate.edu](mailto:Euisseok.Jeong@sdstate.edu) (E. Jeong), [junwon.seo@sdstate.edu](mailto:junwon.seo@sdstate.edu) (J. Seo), [james.p.wacker@usda.gov](mailto:james.p.wacker@usda.gov) (J.P. Wacker).

<sup>1</sup> <https://orcid.org/0000-0001-6046-9319>.

<sup>2</sup> <https://orcid.org/0000-0002-5911-3726>.



**Fig. 1.** Selected UAVs: (a) DJI Phantom 4 and (b) DJI Matrice 210.

2018). For instance, Park et al. (2019) applied Convolutional Neural Network (CNN)-based machine learning to detect cracks on the roadway with inspection images extracted by dash-mounted cameras in vehicles. Two different trained CNN models were used for crack detection. The first CNN model was trained to identify the roadway. With the first CNN results, the images were amended by excluding areas that were not fully recognized between roads and cracks. The amended areas were utilized to detect cracks on the roads from the second CNN training. It was reported that the CNN-based damage classification increased the efficiency of damage detection and classification effortlessly.

The last issue is the imprecise quantification of damage when using UAVs for bridge inspection. Though image quality improvement is completed for damage identification, there is a limitation on the damage quantification to measure the actual dimension of the damage. Actual dimensional sources (i.e., specific length per pixel) are not included in most images. To address this issue, several studies (Duque, Seo, & Wacker, 2018b; Seo, Wacker, & Duque, 2018c) have adopted different image algorithms such as pixel-based measurement. Specifically, Duque, Seo, and Wacker (2018b) conducted a pixel-based measurement using inspection images captured by a UAV and measured the actual length and thickness of cracks by calculating the relative length using the number of the pixels between edge points and the reference length such as deck depth.

This paper is intended to propose a new UAV-aided bridge inspection protocol incorporating CNN-based machine learning with improved visibility images. To check the feasibility of the protocol, two indoor inspections and one on-site inspection were carried out utilizing two UAVs. Using the UAV images captured during each of the inspections, image visibility and quality improvement, damage identification and classification and damage quantification were completed. This paper consists of six sections, including the current section. In the second section, the details for two selected UAVs are provided, and the proposed protocol is described in the third section. The fourth and fifth sections deal with the indoor inspections that were completed for concrete columns and Cross-Laminated Timber (CLT) beams and on-site inspection for an in-service bridge located in Minnesota, U.S. The last section presents the quantifiable findings and collective conclusions supported by this work.

## 2. Selected UAVs

For this study, two UAVs, including DJI Phantom 4 (see Fig. 1a) and DJI Matrice 210 (see Fig. 1b), were utilized to conduct visual indoor and on-site inspections for various structural components and a bridge. Matrice 210 equipped with Zenmuse X5S, which is a high-resolution image sensor, was used for the open space like a bridge, in particular. Zenmuse X5S can collect images with 20.8 megapixels and can also record videos with 4 k digital cinema initiatives ( $4096 \times 2160$ ) using a 17.30 mm width  $\times$  13.00 mm height, 4/3 type, Complementary Metal-

**Table 1**  
Selected UAVs specification.

UAV	DJI Phantom 4	DJI Matrice 210	
Dimension (mm)	$290 \times 290 \times 196$	$887 \times 880 \times 378$	
Weight (kg)	1.38	4.57	
Payload (kg)	0.46	1.57	
Max. speed (m/s)	20	18	
Hovering time (min)	28	13	
Max. wind resistance (m/s)	10	12	
Camera	Sensor Pixels Video resolution	1/2.3" CMOS 12.4 Mega UHD: $4096 \times 2160$ 4 K: $3840 \times 2160$ 2.7 K: $2704 \times 1520$ FHD: $1920 \times 1080$ HD: $1280 \times 720$ Video format MP4, MOV	4/3" CMOS 20.8 Mega 4 K DCI: $4096 \times 2160$ 2160 4 K Ultra HD: $3840 \times 2160$ 2.7 K: $2720 \times 1530$ FHD: $1920 \times 1080$ RAW, ProRes, MOV, MP4
Supported mounts for sensors	Single upward Single downward Dual downward	Not applicable Applicable Not applicable	Applicable Applicable Applicable
Remote range (km)	5.0	7.0	

Oxide Semiconductor (CMOS) camera sensor. In addition to Matrice 210, Phantom 4 was also selected for both inspections at inaccessible areas such as underneath the deck due to its compact size. Phantom 4 can capture images with 12.4 megapixels and record videos with ultra-high definition resolution ( $4096 \times 2160$ ) using a 6.17 mm width  $\times$  4.56 mm height, 1/2.3 type, CMOS camera sensor. Specifications of both UAVs are provided in Table 1.

## 3. UAV-aided inspection protocol

The UAV-aided inspection protocol integrated with CNN-based machine learning and improved visibility images was introduced. This protocol was applied to a total of three inspections: two indoor inspections at South Dakota State University (SDSU) and an on-site bridge inspection in Pipestone, Minnesota (MN). This protocol is detailed in the flowchart as shown in Fig. 2. To evaluate the practicability of the protocol, indoor inspections were initially performed with the selected UAVs as preliminary inspections. With images acquired from the indoor inspections, digital image processing in conjunction with CNN-based machine learning was conducted using image analysis to identify and quantify any damage on the inspected structural components. For the

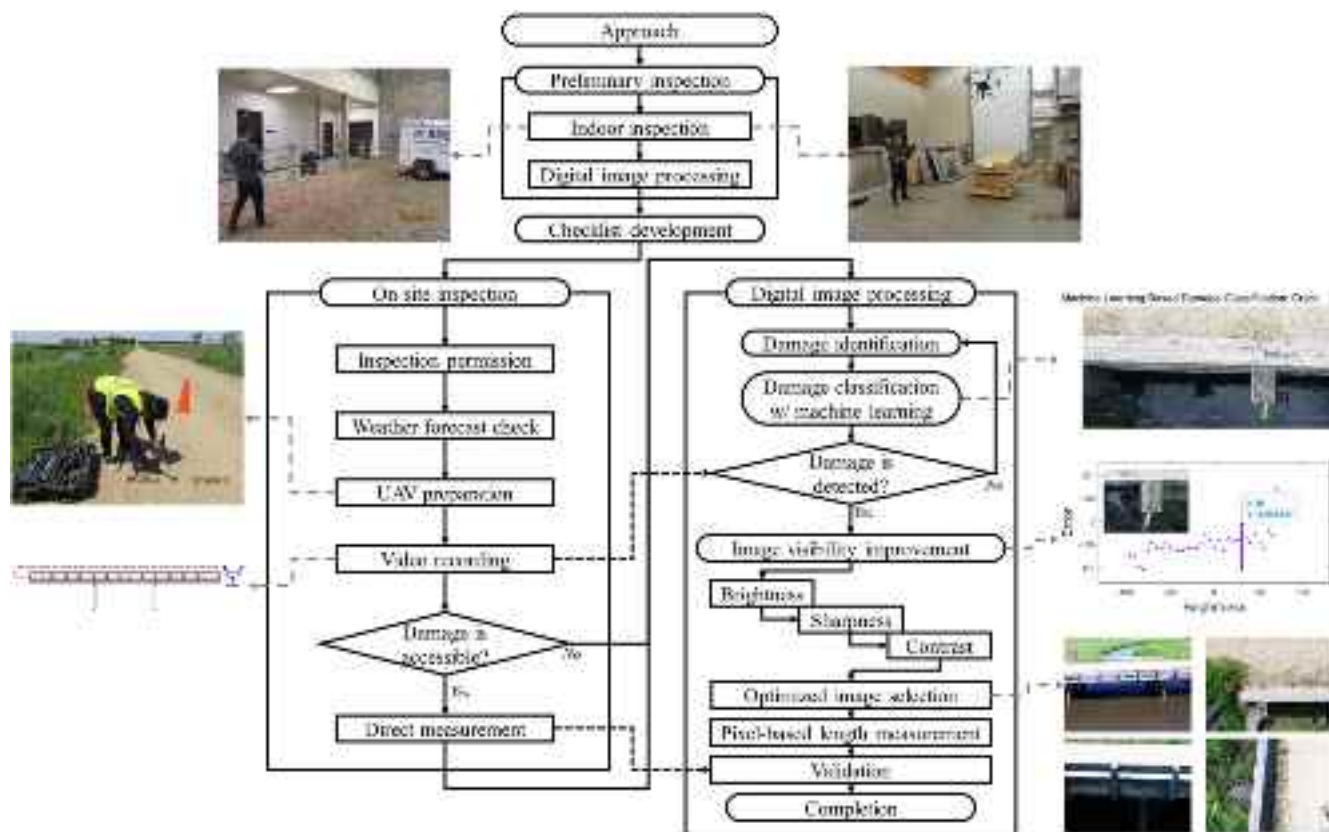


**Fig. 2.** Flowchart of bridge inspection and damage quantification.

damage identification, image visibility improvement techniques were applied to facilitate the adjustment of brightness-contrast-sharpness of UAV raw images. With the processed images, damage quantification was carried out by the pixel-based length measurement algorithm. This algorithm counts the pixels in the image. As the counted number of pixels

is a relative value, the reference length (e.g., structural component) is utilized for the damage measurement using the ratio of pixel number and length. The measured damage size was compared with the direct measurement made using a measuring tape and Vernier caliper to ensure the possible use of the protocol in the on-site bridge. Based on the indoor



**Fig. 3.** Inspected concrete columns during indoor inspections.

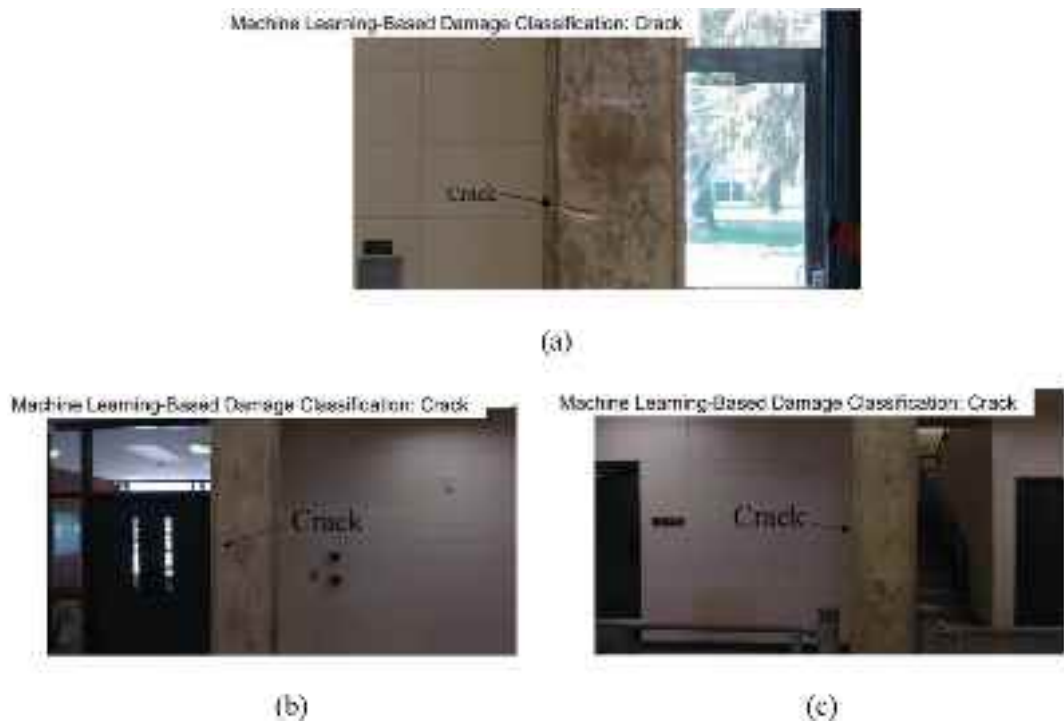


**Fig. 4.** Damage classification using CNN-based machine learning: (a) column A; (b) column B; and (c) column C.

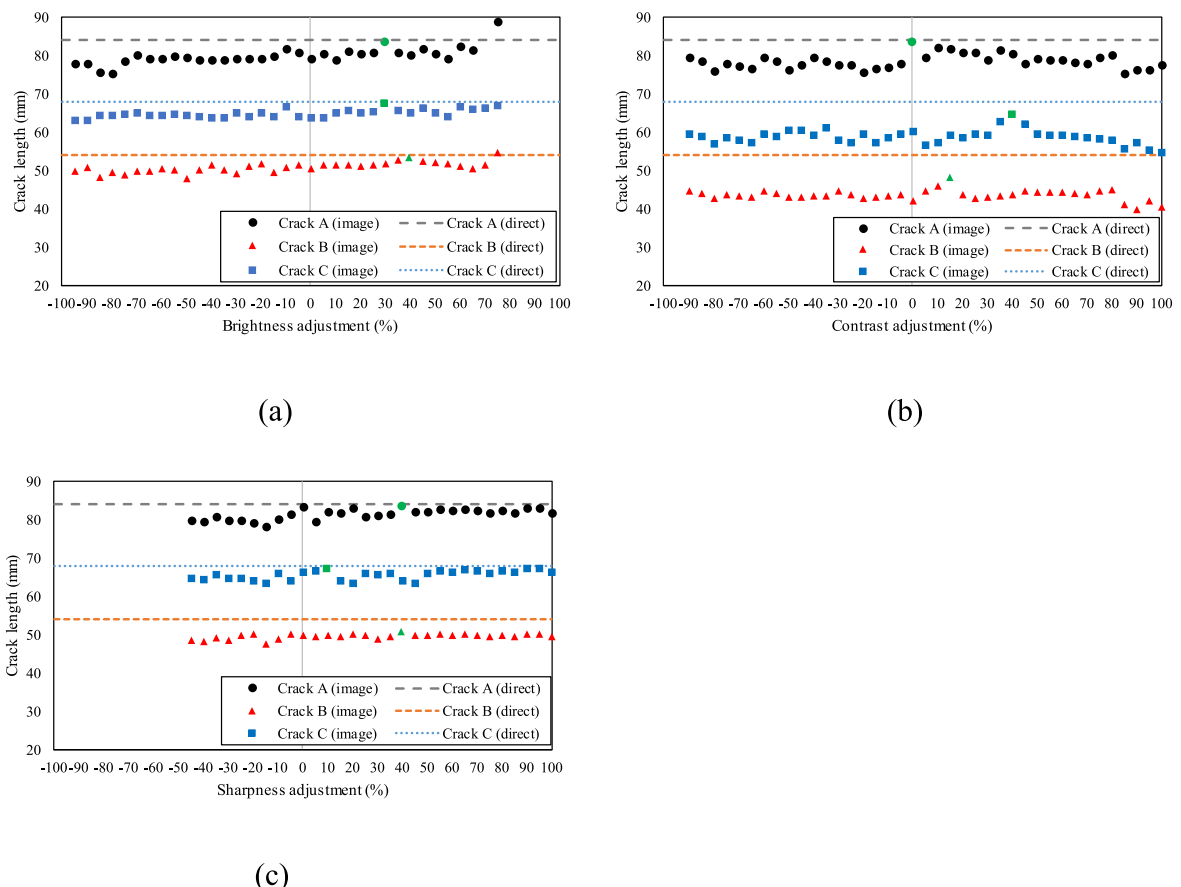


**Fig. 5.** Accuracy of the image analysis-based crack measurement with variation in brightness, contrast, and sharpness: (a) brightness adjustment for crack length; (b) contrast adjustment for crack length with the optimized brightness; and (c) sharpness adjustment for crack length with the optimized brightness and contrast.

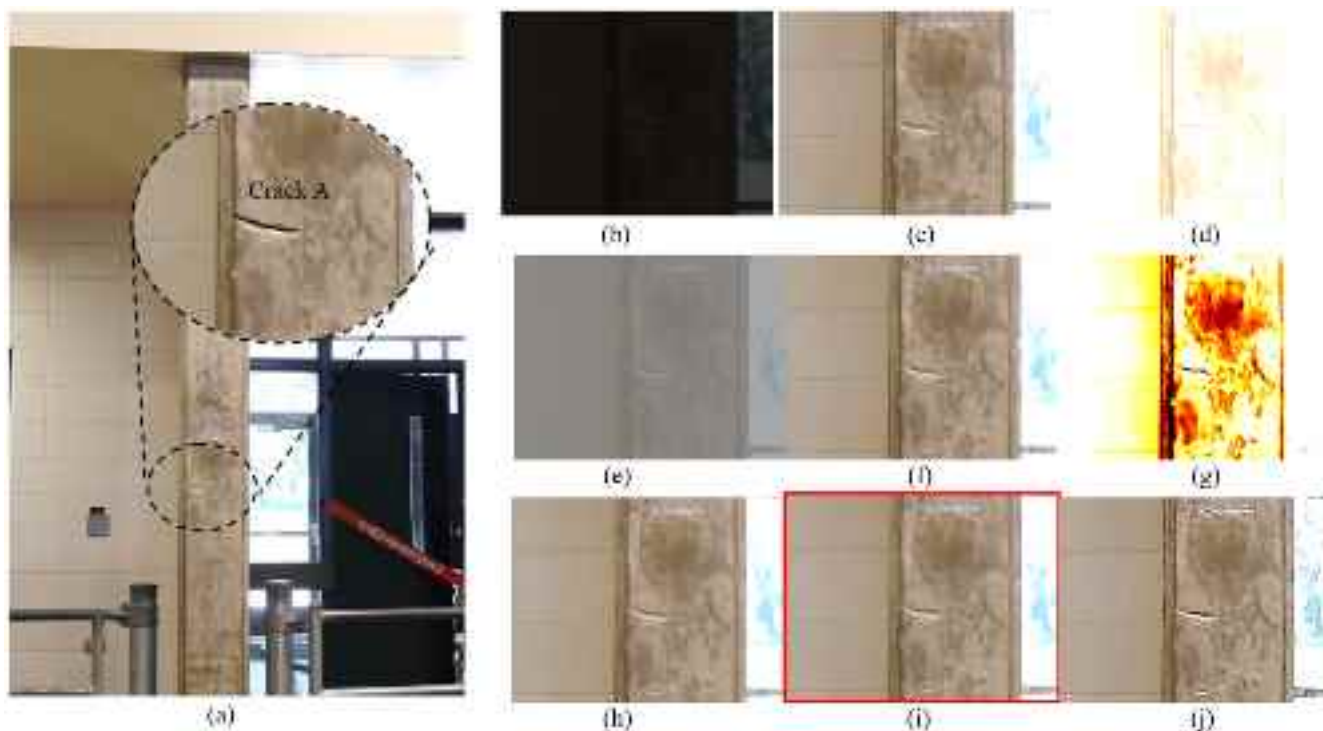


**Fig. 6.** Variation of images adjusted with brightness, contrast, and sharpness: (a) unfiltered crack image on column A; (b) filtered image with brightness  $-75\%$ ; (c) filtered image with brightness  $30\%$  (optimization for brightness); (d) filtered image with brightness  $70\%$ ; (e) Fig. 6c adjusted with contrast  $-75\%$ ; (f) Fig. 6c adjusted with contrast  $0\%$  (optimization for brightness and contrast); (g) Fig. 6c adjusted with contrast  $90\%$ ; (h) Fig. 6f adjusted with sharpness  $-25\%$ ; (i) Fig. 6f adjusted with sharpness  $40\%$  (optimization for all image properties); and (j) Fig. 6f adjusted with sharpness  $90\%$ .

inspection experience, a checklist for UAV-aided bridge inspection was developed. This checklist means all devices necessary for UAV-aided bridge inspection and direct measurement for the bridge. Included in the checklist are, as a minimum, a measuring tape, Vernier caliper, digital camera, checking weather, update, memory storage, and so on.

After the completion of preliminary inspections, the on-site inspection of the in-service bridge was conducted. This inspection was also completed step-by-step following the flowchart as shown in Fig. 2. With inspection images collected by UAVs, the CNN algorithm was employed for efficient damage identification and classification. This algorithm can efficiently classify damage type based on training sets, which have been accumulated and grouped in each type of damage such as discoloration, crack, rust, spalling, and efflorescence. Then, the image visibility improvement technique as used in the preliminary inspections were also employed to improve damage visibility. This technique initially adjusted three basic properties (including brightness, contrast, and sharpness) of the UAV images to improve damage visibility as the first step. A trial-and-error evaluation for damage visibility with UAV images was performed considering variability in each of the basic properties. The evaluation involved the calculation of percent errors between damage quantified from the adjusted images and direct measurements. From this technique, the optimized images can be selected and used to measure damage by analyzing them using the pixel-based measurement algorithm. Damage measured from the image analysis and direct measurement is compared to validate the accuracy of UAV-aided inspection for accessible damage only where direct measurement for the damage is possibly made during the on-site inspection.

#### 4. Preliminary inspections

Before execution of the field inspection of the bridge, indoor inspections with the selected UAVs were conducted as a preliminary inspection in Animal Science Arena and Structure Lab in Crothers

Engineering Hall at SDSU. Damage quantification was also performed using the inspection images acquired from the UAVs. Findings from the indoor inspection are discussed in the subsections below.

##### 4.1. Concrete column inspection

In the first indoor inspection, UAVs captured 24,867 images of columns A through C in Animal Science Arena to identify any damage as displayed in Fig. 3. The images of the columns were examined in detail and a total of three noticeable cracks were visually observed on columns A through C. The damage classification using CNN-based machine learning coupled with the Residual Networks having 50 layers through MATLAB, 2020 was made as shown in Fig. 4 for three cracks on each of the columns.

Upon completion of UAV-aided inspections, the cracks on the columns were also measured directly using a measuring tape, and the direct measurements were compared to those obtained from image analysis of UAV inspection images to examine the accuracy of the UAV-aided inspection protocol. It should be noted that UAV inspection images filtered by adjusting their brightness, contrast, and sharpness were initially used for the image analysis-based crack quantification. Fig. 5 shows the accuracy of damage quantification through the image analysis with the filtered UAV images. The error percentages calculated between the direct measurements and corresponding values obtained from the image analysis with the filtered images with variance in brightness, contrast, and sharpness are illustrated in Fig. 5a through 5c, respectively. In Fig. 5a, dashed lines indicate the direct measurement of column A crack (gray line), B (orange line), and C (blue line), individually, and black circles for column A crack, red triangles for column B crack, and blue boxes for column C crack are defined as the results from the image analysis specific to brightness adjustment. The values having the lowest error against direct measurement are marked with green dots. Similar to Fig. 5a, b and c show the accuracy of contrast and sharpness adjustment,

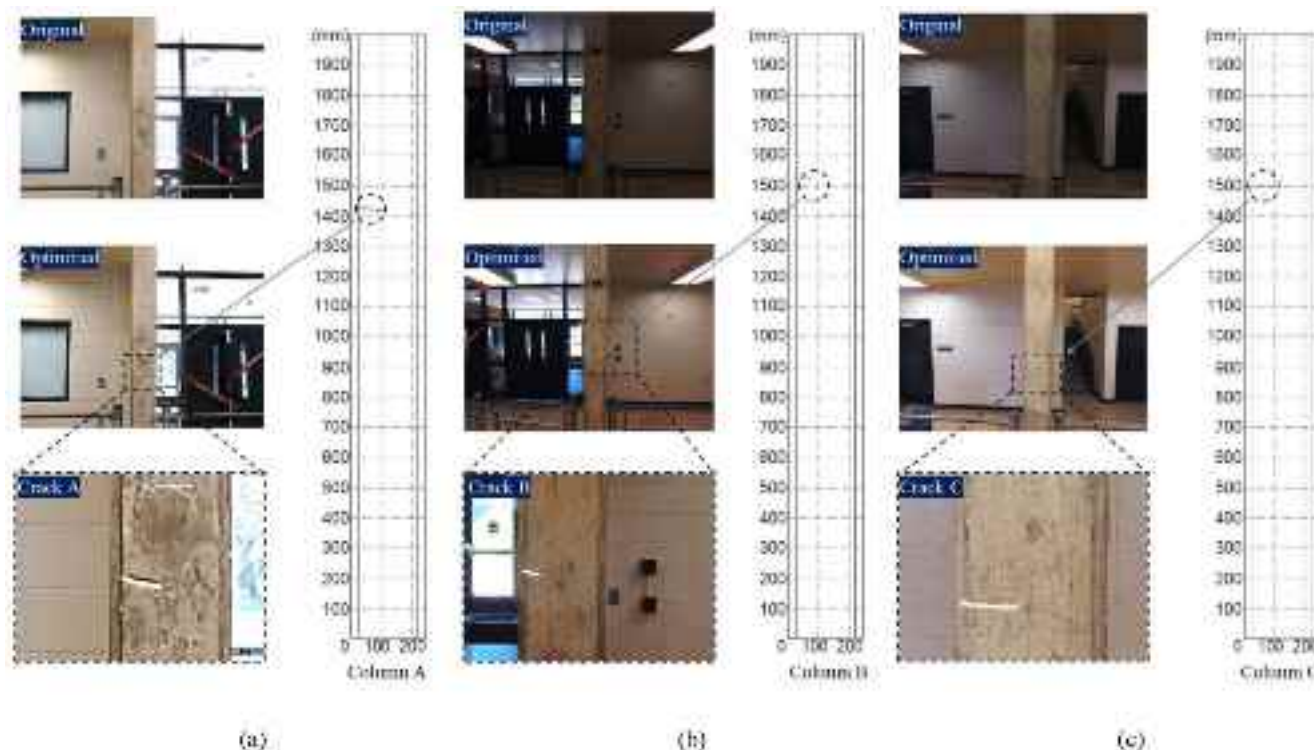


**Fig. 7.** Visual damage maps: (a) column A; (b) column B; and (c) column C.

correspondingly.

The trial-and-error evaluation with brightness, contrast, and sharpness adjustment can be done with the unfiltered UAV images to identify the improved visibility image called “an optimized image” as shown in Fig. 6. Fig. 6a shows the unfiltered UAV image of crack on column A. Image properties (i.e., brightness, contrast, and sharpness) can be adjusted from -100% to 100% with its initial value being 0%. For instance, when the brightness of the UAV image was adjusted between -100% to -80%, the crack was not identified due to darkness under the brightness of -75% as shown in Fig. 6b. The crack was also not observed when the brightness of the UAV image was adjusted between 90% and 100% due to overexposure. The crack (refer to Fig. 6c) was observed clearly when the brightness was adjusted between 30% and 50%, whereas the error of damage quantification was found to be 0.53% deemed as the least value when the UAV image was adjusted with 40% brightness (green circle) as displayed in Fig. 5a. With the improved visibility image adjusted with brightness, contrast adjustment was also conducted as depicted in Fig. 5b. The UAV image with 0% contrast showed the lowest percentage error (green circle) against direct measurement and was considered the contrast-based improved visibility image (see Fig. 6f). The sharpness of Fig. 6f was further adjusted to obtain the optimized image as shown in Fig. 5c. The UAV image adjusted with 40% sharpness showed the optimized image through this procedure as displayed in Fig. 6i.

Fig. 7a, b, and c show the unfiltered UAV inspection images, the optimized images, and corresponding damage maps for columns A, B, and C cracks, respectively. The unfiltered UAV inspection images are shown in Fig. 7a through 7c at the top left for each. After the image visibility improvement technique with the adjustment of image properties was applied to all the images to each of the columns, the following optimized inspection images were obtained: 1) column A crack image with the brightness of 30%, contrast of 0%, and sharpness of 40%; 2) column B crack image with the brightness of 40%, contrast of 20%, and sharpness of 40%; and 3) column C crack image with the brightness of 30%, contrast of 10%, and sharpness of 20%. To better observe damage, the magnified images for each crack are provided as well in these

#### Machine Learning-Based Damage Classification: Crack



**Fig. 8.** Sample of damage classification using machine learning.

figures. From the damage quantification with the optimized images, an average error of 2.56% of image analysis-based measurement was calculated against the direct measurement of the crack length of column A, B, and C cracks.

#### 4.2. CLT beam inspection

As the second indoor inspection, DJI Matrice 210 acquired 7,459 images of CLT beams with a visible crack in the Structure Lab at SDSU to double-check if the proposed protocol was able to identify and quantify the damage on the CLT. Among the acquired images, a UAV inspection image showing the crack on the CLT beams was found through the CNN algorithm as shown in Fig. 8. The UAV image with the crack (refer to Fig. 9a) was adjusted in terms of brightness, contrast, and sharpness as displayed in Fig. 9c through 9k. The trial-and-error evaluation with brightness, contrast, and sharpness variations was performed with the unfiltered and adjusted UAV images to identify the optimized image showing the least error of crack length against the direct measurement as shown in Fig. 9b. In this figure, the black circles, red triangles, and blue boxes indicate the measured crack lengths corresponding to

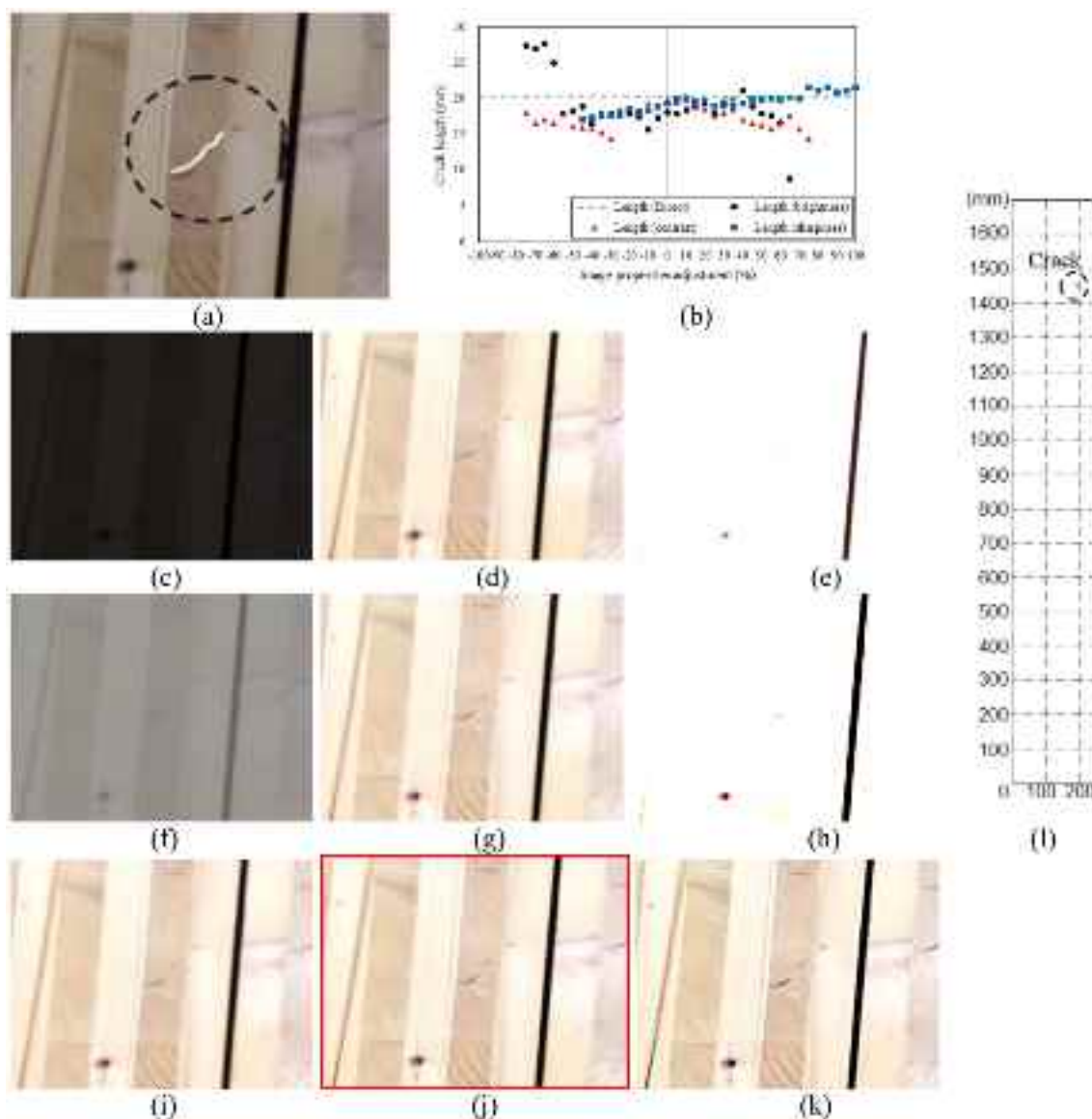


**Fig. 9.** Variation of images adjusted with brightness, contrast, and sharpness: (a) unfiltered crack image on CLT beam; (b) variation in crack size corresponding to brightness, contrast, and sharpness; (c) filtered image with brightness -75%; (d) filtered image with brightness 35% (optimization for brightness); (e) filtered image with brightness 65%; (f) Fig. 9c adjusted with contrast -80%; (g) Fig. 9c adjusted with contrast 10% (optimization for brightness and contrast); (h) Fig. 9c adjusted with contrast 80%; (i) Fig. 9f adjusted with sharpness -50%; (j) Fig. 9f adjusted with sharpness 65% (optimization for all image properties); (k) Fig. 9f adjusted with sharpness 100%; and (l) visual damage map for CLT beam.

brightness, contrast, and sharpness, respectively.

Again, Fig. 9c through 9k show the images according to the adjustment of brightness, contrast, and sharpness. The effect of brightness in the image is observed in Fig. 9c through 9e, and Fig. 9d shows the optimized image adjusted with the brightness of 35%. The crack was not observed in Fig. 9d and f due to darkness and over-illumination, respectively. With Fig. 9d, contrast adjustment was performed as displayed in Fig. 9f through 9h. During the contrast adjustment, the contrast of 10% (see Fig. 9f) exhibited the lowest error against direct measurement as shown in Fig. 9b, whereas the crack was not observed visually in Fig. 9f and h due to inappropriate contrast adjustment. Finally, with Fig. 9g, the optimized image was obtained by adjusting the sharpness to 65 % as shown in Fig. 9j. As Fig. 9i adjusted with the sharpness of -50% has unclear crack edges, this figure is improper for this image visibility improvement technique. On the other hand, Fig. 9k that was adjusted with the sharpness of 100% shows the crack clearly, but other edges are not clear due to over contrast. Using the optimized

image, the damage quantification that was performed revealed an average error of 5.47% against direct measurement, and a corresponding damage map was created as shown in Fig. 9l.

## 5. Studied bridge

A field study of UAV-aided inspection for the bridge located in Pipestone, MN was conducted. This bridge, which was built in 1987, is a four-span timber bridge with a total structure length of 31.7 m, a maximum span length of 7.9 m, and a deck width of 9.1 m. According to the NBI condition rating scale (FHWA, 2018, 1995, 2012), the deck, superstructure, and substructure were recently evaluated in 2017 (FHWA, 2017) and assigned condition ratings of 6 (satisfactory), 6, and 5 (fair), respectively.



**Fig. 10.** Photograph of the inspected bridge taken by Matrice 210.

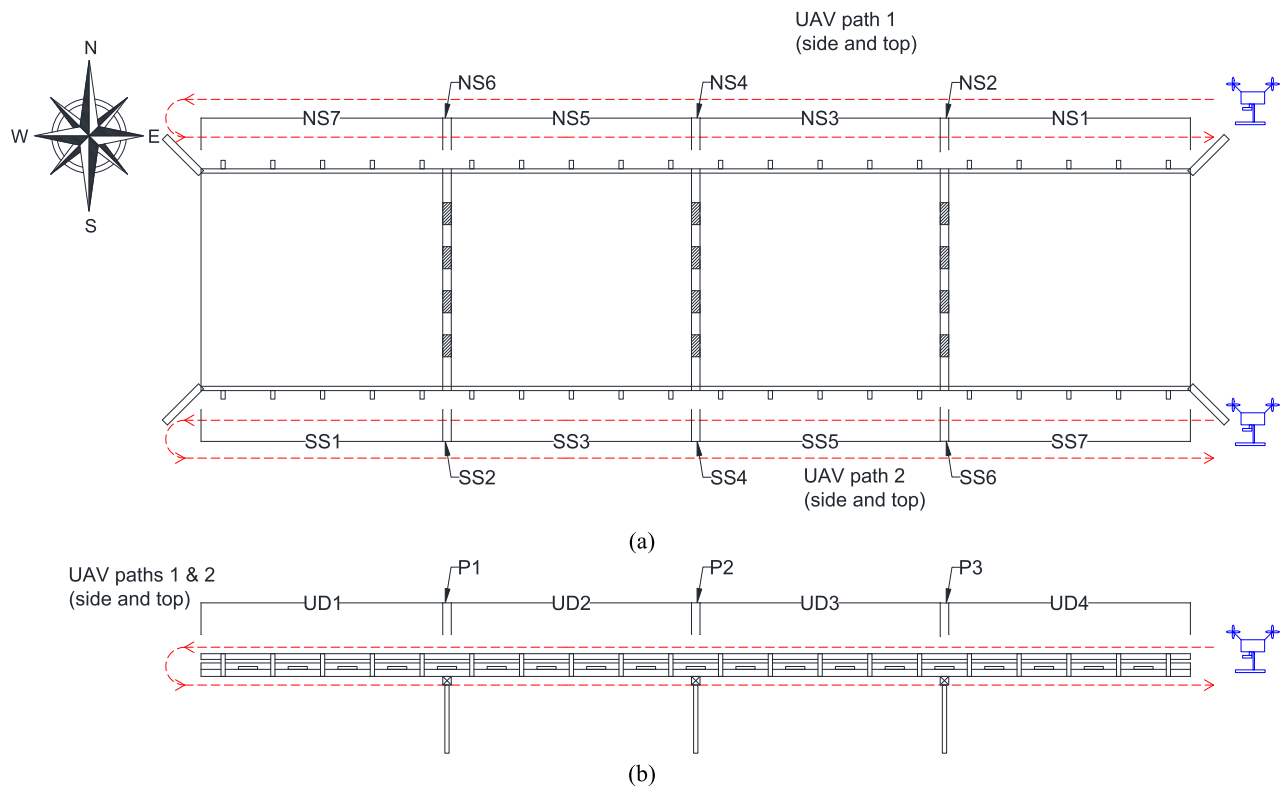


**Fig. 11.** Four-span timber girder bridge sketch with inspected sections: (a) plan view and (b) elevation view.

### 5.1. Prior inspection

Prior to the inspection, appropriate authorizations for the bridge inspection are required from the bridge owner; and thereby, the bridge inspection was approved by Pipestone County, Minnesota. According to the local weather forecast channel (UAV ForecastTM, 2019) on the bridge site, it was a sunny day with an average and maximum wind speed of 2.88 m/s and 6.17 m/s, respectively. The weather conditions forecast for the inspection day were considered satisfactory to operate

the UAVs for the bridge inspection as shown in Fig. 10. The UAVs and supplementary items, encompassing full-charged batteries, a gimbal camera, digital camera, safety items (e.g., traffic cones, hard hats, safety vest, etc.), and direct measurement equipment (i.e., a measuring tape and Vernier caliper) were prepared before the inspection. Note, traffic cones were only installed to secure the takeoff and landing area of the UAVs without any specific traffic control required to mitigate traffic impacts during the inspection.

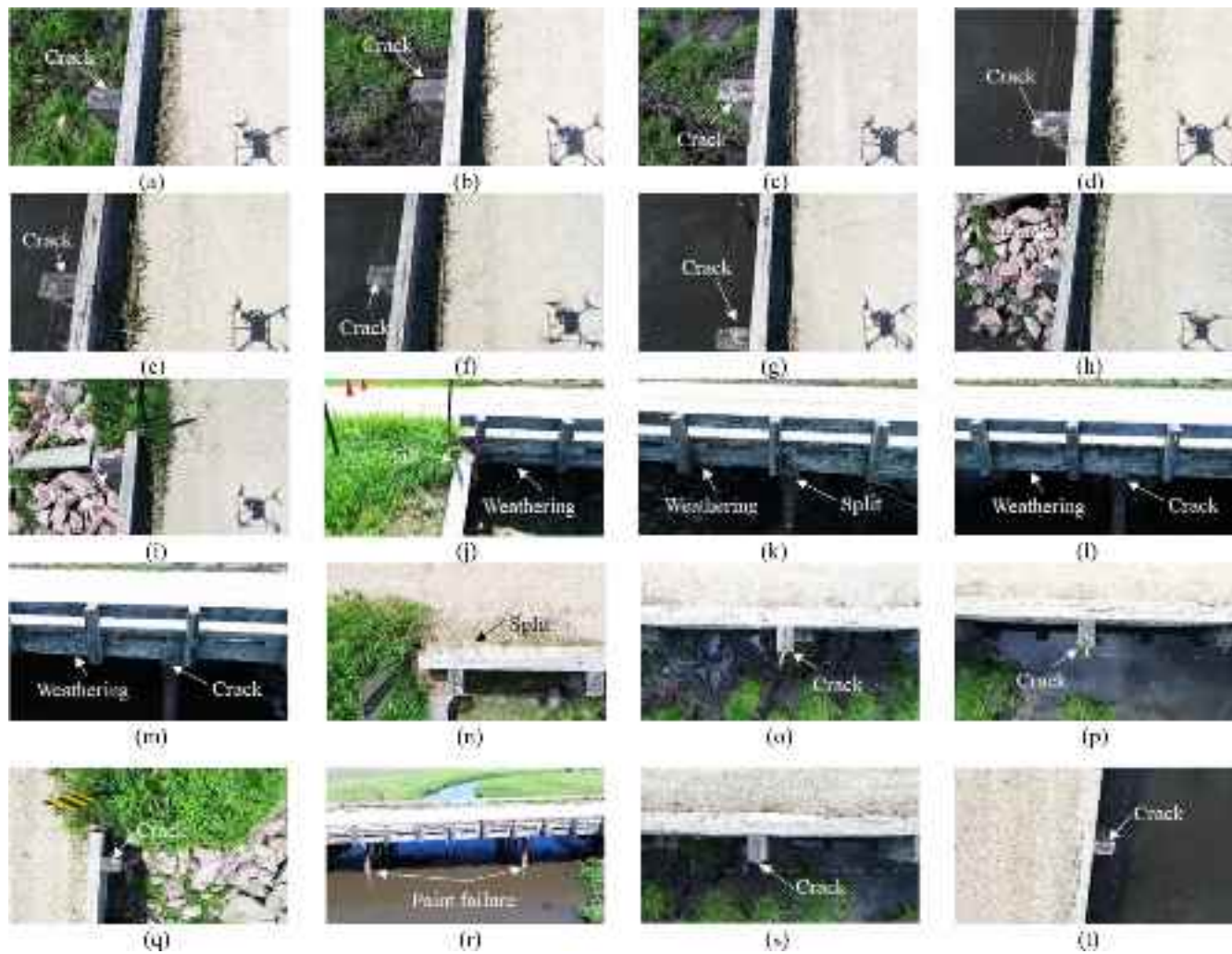
A sketch for this bridge was generated as shown in Fig. 11, including



Fig. 12. Representative damage image showing damage classification result.



Fig. 13. Classified damage using UAV images: (a) crack on the railing on SS1; (b) crack on the railing on SS1; (c) crack on the railing on SS3; (d) crack on the railing on SS3; (e) crack on the railing on SS5; (f) crack on the railing on SS5; (g) crack on the railing on SS5; (h) crack on the railing on SS7; (i) crack on the railing on SS7; (j) tilt and weathering on NS1; (k) weathering and split on NS3; (l) weathering and crack on NS5; (m) weathering and crack on NS7; (n) split on NS1; (o) crack on the railing on SS1; (p) crack on the railing on NS1; (q) crack on the railing on NS7; (r) paint failure on NS; (s) crack on the railing on NS5; and (t) crack on the railing on NS5.



**Fig. 14.** Optimized UAV inspection images adjusted with the brightness of 20%, contrast of 20%, and sharpness of 30%; (a) crack on the railing on SS1; (b) crack on the railing on SS1; (c) crack on the railing on SS3; (d) crack on the railing on SS3; (e) crack on the railing on SS5; (f) crack on the railing on SS5; (g) crack on the railing on SS5; (h) crack on the railing on SS7; (i) crack on the railing on SS7; (j) tilt and weathering on NS1; (k) weathering and split on NS3; (l) weathering and crack on NS5; (m) weathering and crack on NS7; (n) split on NS1; (o) crack on the railing on SS1; (p) crack on the railing on NS1; (q) crack on the railing on NS7; (r) paint failure on NS; (s) crack on the railing on NS5; and (t) crack on the railing on NS5.

the plan view (Fig. 11a) and elevation view (Fig. 11b). Specifically, for effective damage identification, the superstructure of the bridge is divided into seven sections on each side as shown in Fig. 11a. In this figure, NS represents the north side of the bridge, and SS indicates the south side of the bridge. As shown in Fig. 11b, underneath the bridge deck is also divided into seven individual sections, including UD1 through UD4, and the bridge pier sections are denoted as P1 through P3. Note, UD indicates underneath deck and P is defined as a pier. The UAV-aided bridge inspection was conducted by following UAV paths 1 and 2 as depicted in Fig. 11. Each UAV path includes inspection of the side of the bridge and top of the railings.

## 5.2. Damage identification

During the UAV flight, the UAVs recorded videos considered as an appropriate image acquisition method to avoid any omission of images possessing damage. A total of 28,614 images extracted from the 8 inspection videos were used for damage identification following the proposed protocol. During the damage identification, the damage was classified using CNN-based machine learning as shown in Fig. 12. This figure shows the sample image with the crack detected from the CNN-based damage classification. As a result of the CNN application, crack

(see Fig. 13a through 13i, 13o, 13p, 13q, 13s, and 13t), weathering (refer to Fig. 13j, 13l, and 13m), split (see Fig. 13k and 13n), and paint failure (refer to Fig. 13r) were initially classified. Note, a small box (top-left) in each figure indicates the results of CNN-based damage classification. “C” with red box indicates crack, “W” with the orange box represents weathering, “S” with green box indicates split, and “P” with purple box shows paint failure.

Upon the completion of CNN-based damage classification, various types of damage including crack (see Fig. 13a through 13i, 13l, 13m, 13o, 13p, 13q, 13s, and 13t), split (see Fig. 13k and 13n), tilt (see Fig. 13j), and paint failure (see Fig. 13r), and weathering timbers (refer to Fig. 13j through 13m) were further investigated manually from each of the UAV images to ensure that the CNN-based damage classification was able to identify individual damage types correctly. It is important to note that because the applied CNN algorithm was only capable of showing one damage classification result, another damage classification was not provided in the inspection images having more than one damage (i.e., Fig. 13j through 13 m). With the UAV images in Fig. 13, image properties’ adjustment with the brightness of 20%, contrast of 20%, and sharpness of 30% was performed as shown in Fig. 14. Through this algorithm, the visibility of the inspection images was improved as in the process with indoor UAV inspection images. For instance, weathering in

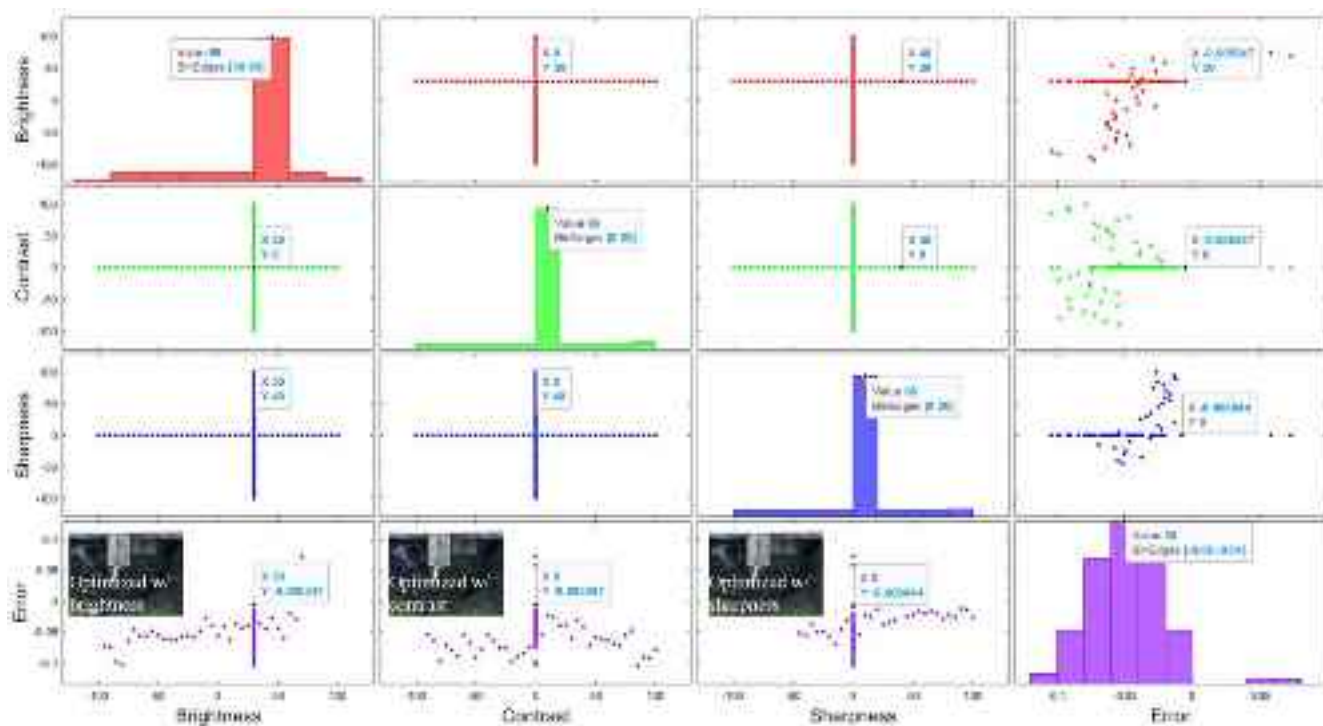


**Fig. 15.** Graphical representation for variation in accuracy of image analysis-based damage quantification corresponding to brightness, contrast, and sharpness along with errors.

darkness (Fig. 13j through 13 m) can be observed undoubtedly as depicted in Fig. 14j through 14 m.

### 5.3. Damage quantification

Accessible damage and reference dimensions required for the damage quantification through the image analysis were measured by hand and recorded during the UAV inspections. To measure the size of the damage in the inspections, the image size was calculated by counting the number of pixels covering the damage in each image using ImageJ, image analysis software, that can measure the damage size from the image. It should be noted that a reference dimension (e.g., length of a railing post) was also used for the image analysis. As part of the proposed protocol, this process was applied to each of the images that were classified by the CNN algorithm per damage type to measure corresponding damage. Upon completion of the process, the optimized images were obtained per damage type.

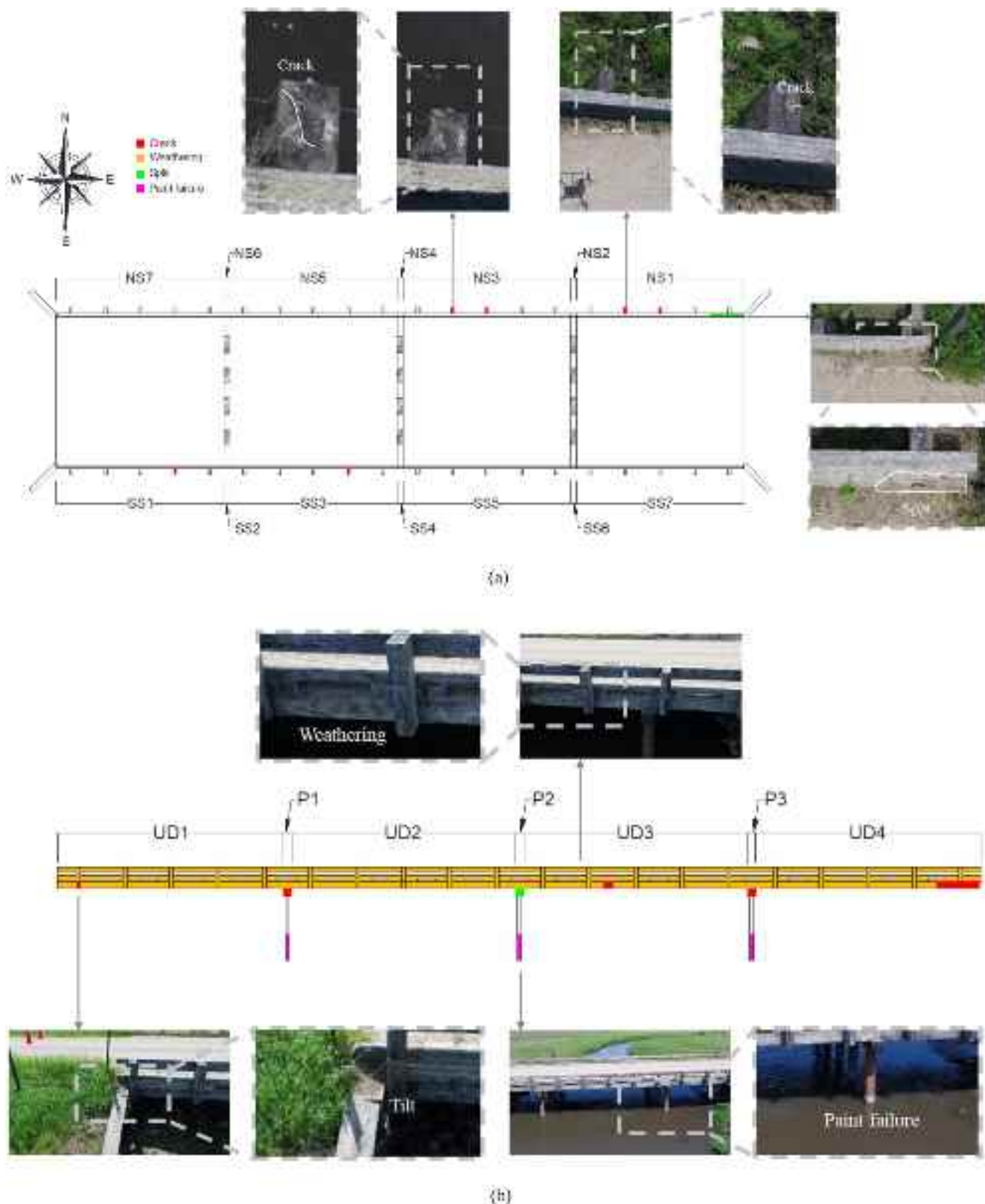
For example, with a visible crack on the railing post, the accuracy of image analysis-based damage quantification was evaluated as shown in Fig. 15. The crack on the railing post was measured taking account into the image properties' variations. The UAV inspection image used for the crack quantification was adjusted with brightness of 30%, contrast of 0%, and sharpness of 0%. Note, this image was considered as the optimized image that shows an average error of 2.92 % only against the direct measurement. This figure includes the 12 scatter and 4 histogram charts created by considering the variability in brightness, contrast, and sharpness of the optimized image. As an example of explanations for these charts, the red histogram chart for brightness shows a mode at brightness between 30 and 60 and 88 defined as the number of data points within the brightness range. Similarly, the green and blue histograms for contrast and sharpness have an identical mode and data point number between 0 and 20. Data points in the red, green, and blue scatter charts for combinations of the image properties such as brightness-contrast and brightness-sharpness mean the frequency. As shown at the bottom of Fig. 15, meanwhile, purple charts show the relationship between image property values and errors that were calculated between

image-based damage quantification and direct measurement. In these charts, values of the image properties closest to zero are considered as the optimized image. As an example of these purple charts, error-brightness and error-contrast show the minimum error value of -0.005347 obtained at the brightness of 30% and the contrast of 0%, respectively.

A damage map of the inspected bridge showing all the identified damage and corresponding optimized UAV inspection images is provided as shown in Fig. 16. The UAV images in this figure show different types of damage, including crack, split, weathering, tilt, and, paint peeling off. Note, the optimized images were obtained by performing the image visibility improvement process with the unfiltered UAV images with adjustment of image properties as stated before. The detailed damage descriptions provided from the inspection report completed by the bridge inspector, who are responsible for identifying any defects on the bridge, the quantified damage through the UAV-aided inspection protocol, and the direct measurements for accessible damage are also summarized in Table 2. It is worthwhile to note that the bridge inspectors did not quantify most of the damage. For example, the cracks on the railing posts were described as "all posts have moderate checks present" in the inspection report (Pipistone County, 2018). However, all the damage presented in the inspection report (Pipistone County, 2018) was identified and quantified using the proposed protocol with the inspection images obtained by the UAVs. Based on the comparison with the inspection report, overall, the proposed protocol with UAVs was able to appropriately identify all the damage presented in the report and quantify them through the image analysis. Also, the average error of UAV image analysis-based measurement compared to the direct measurement performed during the inspection showed 9.12%.

## 6. Conclusions

The goal of this paper was to propose Convolutional Neural Network (CNN)-based machine learning in conjunction with improved visibility images acquired by Unmanned Aerial Vehicles (UAVs). Two UAVs, including DJI Phantom 4 and DJI Matrice 210, were used for this work.



**Fig. 16.** Damage map for the studied bridge with representative optimized inspection images: (a) plan view and (b) elevation view.

The proposed protocol was applied for the two indoor inspections and one on-site bridge inspection, in an attempt to evaluate the accuracy and performance in terms of damage identification and quantification. Based on the three applications of the proposed protocol, the following conclusions were made:

1. From the indoor inspections, different sizes of cracks on the column columns and one visible crack on the Cross-Laminated Timber (CLT) beam were efficiently identified through the proposed protocol with CNN-based machine learning.

**Table 2**  
Inspection report.

Bridge component	UAV-aided bridge inspection	Inspection report (2018)	Direct measurement
Deck	35.57 cm long and 0.41 cm wide diagonal crack on north edge laminations in the outer deck panel between west pile cap and center pile cap. Moderate moisture staining is present for the deck North and south sides. There is 1.21 cm gap in NW deck side.	Outside deck timber is diagonally cracked on north edge laminations in the outer deck panel between the west pile cap and center pile cap. Moderate moisture staining is present for the entire deck. There are loose & broken deck timbers by the rail curbs.	Not applicable Moderate moisture staining is present for the entire deck. Not applicable
Railing	All posts have moderate decay. Vertical 12.12 cm crack on 3rd NE post.  Vertical 11.23 cm crack on 4th NE post.  Vertical 7.89 cm crack on 8th NE post.  Vertical 14.32 cm crack on 9th NE post.  Vertical 6.67 cm crack on 4th SW post. Vertical 4.67 cm crack on 9th SE post.	All posts have moderate checks present.  Vertical 13.22 cm crack on 4th NE post.  Vertical 6.97 cm crack on 8th NE post.  Vertical 13.21 cm crack on 9th NE post.  Vertical 7.32 cm crack on 4th SW post. Vertical 5.33 cm crack on 9th SE post.  The 9th post from the west in the south rail has a 0.91 m long hit in the curb that caused a piece to be broken out.	All posts have moderate decay. Vertical 11.31 cm crack on 3rd NE post.  Vertical 13.22 cm crack on 4th NE post.  Vertical 6.97 cm crack on 8th NE post.  Vertical 13.21 cm crack on 9th NE post.  Vertical 7.32 cm crack on 4th SW post. Vertical 5.33 cm crack on 9th SE post.
Pier cap	Split (8.54 cm) on SS2  Crack (13.21 cm) on SS4  Split (11.31 cm) on SS6	All timber caps have small horizontal checks in them.  South end, outside has a check, up to 15.24 cm deep and 1.27 cm wide, where the 2 slabs join together, some movement is present.  North end, west side, has 6.35 cm deep chunks missing.	Not applicable Not applicable Not applicable
Column/pier/pile Floor beam	Paint is starting to peel off. 13.65 cm crack on East beam	Paint is starting to peel off. Beams have horizontal checks.	Not applicable 12.86 cm crack on East beam

- From the on-site bridge inspection, various types of damage, including split, crack, weathering timber, and paint failure, were identified by investigating the UAV images through the CNN-based protocol at a low computational cost.
- Adjustment of brightness, contrast, and sharpness in the indoor and on-site UAV inspection images was found to enhance the visibility of the image quality with damage and the accuracy of the image analysis-based damage measurements.
- The proposed protocol was able to quantify the damage observed in each structural component with an error of 2.56% (cracks on the concrete columns), 5.47% (crack on the CLT beam), and 9.12% (in-service timber bridge) compared to the direct measurements.

## 7. Data availability statement

The data collected from the inspections that support the findings of this study are available from the corresponding author upon reasonable request.

## Declaration of Competing Interest

The authors declare that they have no known competing financial interests or personal relationships that could have appeared to influence the work reported in this paper.

## Acknowledgments

Partial financial support for this research was provided by the United States Department of Agriculture (USDA), Forest Service through Joint Venture Agreement No. 18-JV-11111133-031) and in conjunction with the Forest Products Laboratory (FPL). The assistance and cooperation of the Pipestone County engineers is gratefully acknowledged.

## References

- Cunningham, K., Lattanzi, D., Dell'Andrea, R., Riley, M., Huette, T., Goetz, R., and Wilson, R. (2015). "UAS-Based Inspection of the Placer River Trail Bridge:A Data-Driven Approach." *Structures Congress 2015*, American Society of Civil Engineers, Portland, Oregon, 607–615.
- Dick, K., Russell, L., Dosso, Y. S., Kwamena, F., & Green, J. R. (2019). Deep Learning for Critical Infrastructure Resilience. *Journal of Infrastructure Systems*, 25(2), 05019003.
- Duque, L., Seo, J., & Wacker, J. P. (2018a). Synthesis of Unmanned Aerial Vehicle Applications for Infrastructures. *Journal of Performance of Constructed Facilities*, 32 (4), 04018046.
- Duque, L., Seo, J., & Wacker, J. P. (2018b). Bridge Deterioration Quantification Protocol Using UAV. *Journal of Bridge Engineering*, 23(10), 04018080.
- Federal Highway Administration (FHWA). (1995). *Recording and Coding Guide for the Structure Inventory and Appraisal of the Nation's Bridges* (p. 124). DOT FHWA, Washington, DC: U.S.
- Federal Highway Administration (FHWA). (2017). *National Bridge Inventory (NBI) Data*. USDOT FHWA, Washington, DC: NBI ASCII files.
- FHWA (Federal Highway Administration). (2012). *Recording and Coding Guide for the Structure Inventory and Appraisal of the Nation's Bridges* (p. 124). DOT FHWA, Washington, DC: U.S.
- FHWA (Federal Highway Administration). (2018). *Recording and Coding Guide for the Structure Inventory and Appraisal of the Nation's Bridges* (p. 124). DOT FHWA, Washington, DC: U.S.
- Gervaise, A., Osemont, B., Lecocq, S., Noel, A., Micard, E., Fellinger, J., & Blum, A. (2012). CT image quality improvement using adaptive iterative dose reduction with wide-volume acquisition on 320-detector CT. *European Radiology*, 22(2), 295–301.
- Gulgec, N. S., Takáč, M., & Pakzad, S. N. (2019). Convolutional Neural Network Approach for Robust Structural Damage Detection and Localization. *Journal of Computing in Civil Engineering*, 33(3), 04019005.
- Hallermann, N., & Morgenthal, G. (2014). Visual inspection strategies for large bridges using Unmanned Aerial Vehicles (UAV). In *Proc. of 7th IABMAS, International Conference on Bridge Maintenance, Safety and Management* (pp. 661–667).
- Inoue, A., & Tajima, J. (1994). Adaptive quality improvement method for color images. B. E. Rogowitz and J. P. Allebach, eds., San Jose, CA, 429–439.
- Kao, W., Ye, J., Chu, M., & Su, C. (2009). Image quality improvement for electrophoretic displays by combining contrast enhancement and halftoning techniques. *IEEE Transactions on Consumer Electronics*, 55(1), 15–19.
- Khaloo, A., Lattanzi, D., Cunningham, K., Dell'Andrea, R., & Riley, M. (2018). Unmanned aerial vehicle inspection of the Placer River Trail Bridge through image-based 3D modelling. *Structure and Infrastructure Engineering*, 14(1), 124–136.
- MATLAB. (2020). version 9.9.0. 1538559 (R2020b Update 3). The MathWorks Inc., Natick, Massachusetts.
- Nomura, T., Okamura, M., Nitani, E., & Numata, T. (2008). Image quality improvement of digital holography by superposition of reconstructed images obtained by multiple wavelengths. *Applied Optics*, 47(19), D38.
- Otero, L. D., Gagliardo, N., Dalli, D., Huang, W.-H., & Cosentino, P. (2015). *Proof of Concept for Using Unmanned Aerial Vehicles for High Mast Pole and Bridge Inspections* (p. 170). Florida DOT, Melbourne, FL: Final Report.
- Park, S., Bang, S., Kim, H., & Kim, H. (2019). Patch-Based Crack Detection in Black Box Images Using Convolutional Neural Networks. *Journal of Computing in Civil Engineering*, 33(3), 04019017.
- County, P. (2018). *Minnesota Structure Inventory Report*. Pipestone County: Pipestone County.
- Reagan, D., Sabato, A., & Nizzecki, C. (2017a). *Unmanned aerial vehicle acquisition of three-dimensional digital image correlation measurements for structural health monitoring of bridges* (p. 1016909). Oregon, United States: Portland.

- Reagan, D., Sabato, A., & Niezrecki, C. (2017b). Feasibility of using digital image correlation for unmanned aerial vehicle structural health monitoring of bridges. *Structural Health Monitoring*, 17(5), 1056–1072.
- Seo, J., Duque, L., & Wacker, J. P. (2018a). Field Application of UAS-Based Bridge Inspection. *Transportation Research Record: Journal of the Transportation Research Board*, 036119811878082.
- Seo, J., Duque, L., & Wacker, J. P. (2018b). Drone-enabled bridge inspection methodology and application. *Automation in Construction*, 94, 112–126.
- Seo, J., Wacker, J. P., & Duque, L. (2018c). *Evaluating the use of drones for timber bridge inspection*. General Technical Report FPL-GTR- 258, U.S. Department of Agriculture, Forest Service, Forest Products Laboratory, Madison, WI, 145.
- UAV Forecast<sup>TM</sup>. (2019). “UAV Forecast.” <<http://www.UAVForecast.com>> (Jul. 22, 2019).
- Yang, G., Li, Q. J., Zhan, Y., Fei, Y., & Zhang, A. (2018). Convolutional Neural Network-Based Friction Model Using Pavement Texture Data. *Journal of Computing in Civil Engineering*, 32(6), 04018052.
- Zink, J., & Lovelace, B. (2015). *Unmanned Aerial Vehicle Bridge Inspection Demonstration Project*. MN/RC 2015-40, Minnesota Department of Transportation, Oakdale, MN, 214.